Journal of Materials Science and Nanotechnology
Volume 14 | Issue 1
ISSN: 2348-9812

Review Article Open Access

Study of XPS and Electrical Properties of Strontium-doped Lanthanum Cobaltite (LSC) Thin Films as Cathode for SOFC

Babaso Kamble S[1], Pranav Kamble B[2]

[1]Department of Physics, D.B.J. College, Chiplun-415605, India
[2]Department of Electronic and Instrumentation Science, Savitribai Phule Pune University, Pune- 411007, India

[*]**Corresponding Author:** Department of Physics, D.B.J. College, Chiplun-415605, India, E-mail: kamblebabaso@yahoo.com

Citation: Babaso Kamble S, Pranav Kamble B Study of XPS and Electrical Properties of Strontium-doped Lanthanum Cobaltite (LSC) Thin Films as Cathode for SOFC, J Mater Sci Nanotech nol 14(1): 102

Received Date: July 13, 2026 **Accepted Date:** July 16, 2026 **Published Date:** July 30, 2026

Abstract

The structural properties of La1-xSrxCoO3 with strontium contents of x = 0.1-0.4 mol% have been studied. Strontium--doped lanthanum cobaltite thin films were synthesized using the spray pyrolysis technique (SPT). To confirm phase formation, XRD analysis was performed on these films. The particle size of the sample was measured to be 110.7 nm. X-ray Photoelectron Spectroscopy was used to examine the surface electronic structure of the crystalline thin film. The UV-Vis absorption spectrum of LSC thin films shows high absorption in the ultraviolet region around 230 nm. UV-Vis spectroscopy showed that the band gap increases with higher strontium content. The D. C. electrical resistivity was determined using the two-probe method. An impedance study of LSC samples was conducted, and it was found that space charge polarisation occurs in the samples

Keywords: Spray Pyrolysis, XPS, Hall Effect, Cathode, LSC, SOFC

1. Introduction

The solid oxide fuel cell (SOFC) has promising potential as a clean and efficient energy conservation device for future development. Typically, the operating temperature of SOFCs is 800-1000℃, which limits their use in commercial applications. Therefore, reducing the operating temperature of SOFCs below 600℃ is crucial. Recently, significant progress has been made in lowering the operating temperature of SOFCs from high temperatures to a range of 600-800℃ [1]. The reduction of the operating temperature of SOFCs depends on electrode polarization resistance [2]. The material used for the SOFC cathode played a crucial role in the operating temperature of the SOFC. This is because poor catalytic activity towards oxygen reduction at lower temperatures can reduce performance [3, 4]. To enhance the cathodic performance, SOFC cathode materials are usually composite materials [5]. These cathode materials offer high electronic conductivity, which is important for reducing the operating temperature of SOFC.

We aim to develop cathode materials that exhibit good electronic and ionic conductivity at low operating temperatures. LSC exhibits high catalytic activity at intermediate temperature [6, 7]. Lanthanum Strontium Cobaltite (LSC) should help to develop and maintain cell performance, provide long-term durability, and deliver high conductivity for SOFC [8]. Mixed ionic-electronic conductors can conduct both electrons and ions, making them suitable for SOFCs. Lanthanum cobaltite ($LaCoO_3$) has been identified as a candidate material for SOFCs and is attractive due to its high oxidation power, thermal stability, superconductivity, and excellent catalytic activity [9, 10]. Instead of lanthanum cobaltite, strontium-doped lanthanum cobaltite (LSC) is used, as it offers both mixed ionic-electronic conductivity and acceptable catalytic activity for oxygen reduction, making it suitable for SOFCs [11–14]. The objective of this research is to investigate the structural, spectroscopic, and electrical properties of LSC thin films with varying strontium concentrations. The study aims to elucidate the effect of strontium concentration on these properties.

2. Experimental

X-ray measurements are performed to verify phase formation using a Rigaku Mini Flex 600 X-ray diffract meter with Cu Kα radiation (wavelength 1.5418 Å). The chemical composition in the surface region was investigated by X-ray photoelectron spectroscopy. A two-probe resistivity measurement setup was used to measure the D.C. resistivity and record its variation with temperature. The variation of the real and imaginary components of impedance with frequency for LSC samples at room temperature was measured using an impedance analyzer.

3. Results and Discussion

3.1 XRD Studies

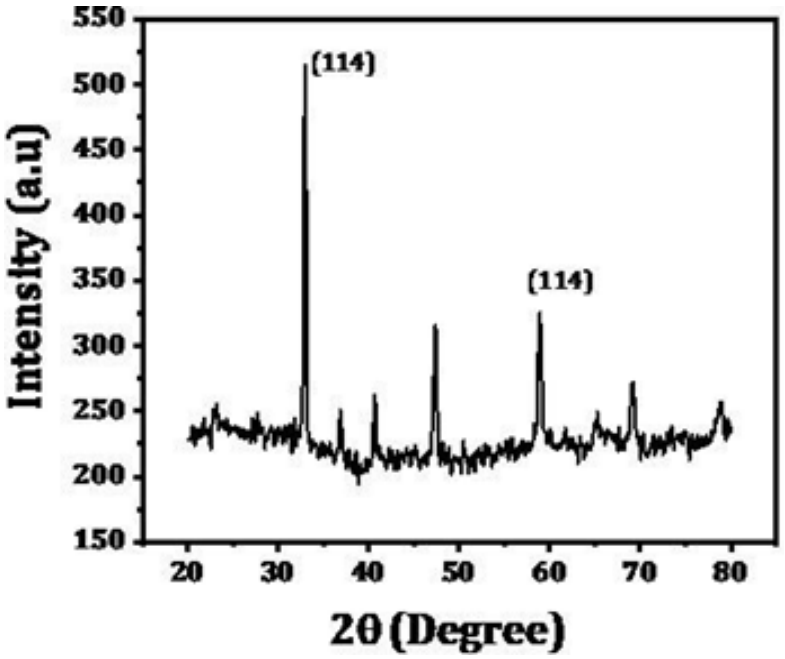

Figure 1. XRD of LSC thin films

(Figure 1) shows the X-ray diffraction pattern of LSC thin films, which were sintered at 1100 ℃ for 2 hours. The most intense XRD peak, which matches the JCPDS file 48-0122, indicates the formation of the perovskite phase. The particle size of the sample is found to be 110.7 nm.

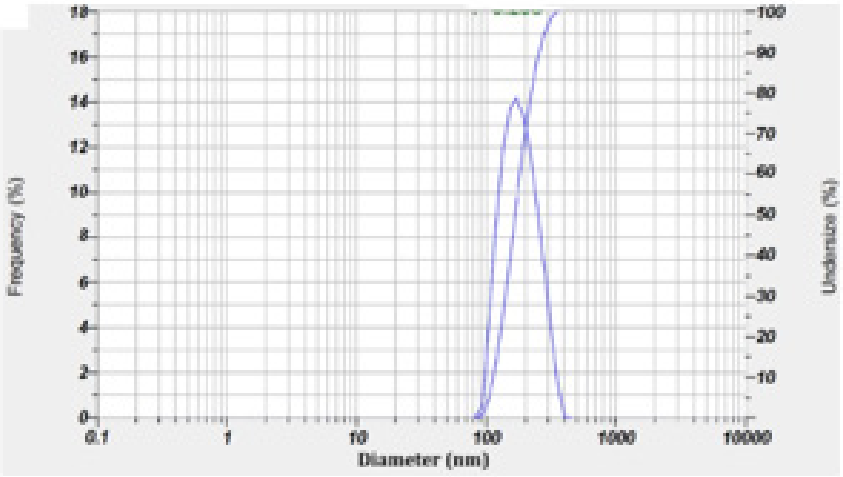

Figure 2. Particle size distribution of LSC thin films

Table 1. Particle Size Distribution

Peak	S. P. Area	Mean	S. D.	Mode
No	Ratio			
1	1	127.5 nm	54.8 nm	110.0 nm
2	----	----	----	----
3	----	----	----	----
Total	1	127.5 nm	54.8 nm	110.0 nm

3.2 X-ray Photoelectron Spectroscopy (XPS)

XPS is an essential tool for examining the surface properties of solid materials [15]. For quantitative analysis of the surface electronic structure of crystalline solids, photoelectron spectroscopy is employed. (Figure 3) shows the XPS spectrum of LSC thin films. The binding energies of La 3d5/2 and Sr 3d5/2 are 839 eV and 139 eV, respectively. This suggests that lanthanum and strontium are in trivalent and bivalent states, respectively [16]. Due to strong spin-orbit interactions, the lanthanum XPS peaks split, as expected for a carbonate, as shown in (Figure 4(a)).

As shown in (Figure 4(c)), the CO (p) spectrum is decomposed into cobalt oxide components at 784.9 eV and 783.7 eV, corresponding to CO 2p3/2 and Co 2p1/2, respectively. The CO 2p3/2 spin-orbit doublet can be deconvoluted into two peaks at 783.9 eV and 783.7 eV, assigned to CO3+ 2p3/2 and CO2+ 2p3/2, respectively. The CO 2p1/2 spin-orbit doublet can also be deconvoluted into two distinct peaks at 783.9 eV and 783.7 eV, assigned to CO3+ 2p1/2 and CO3+ 2p3/2, respectively. In (Figure 4(e)), the binding energy peak at 531 eV could be assigned to oxygen.

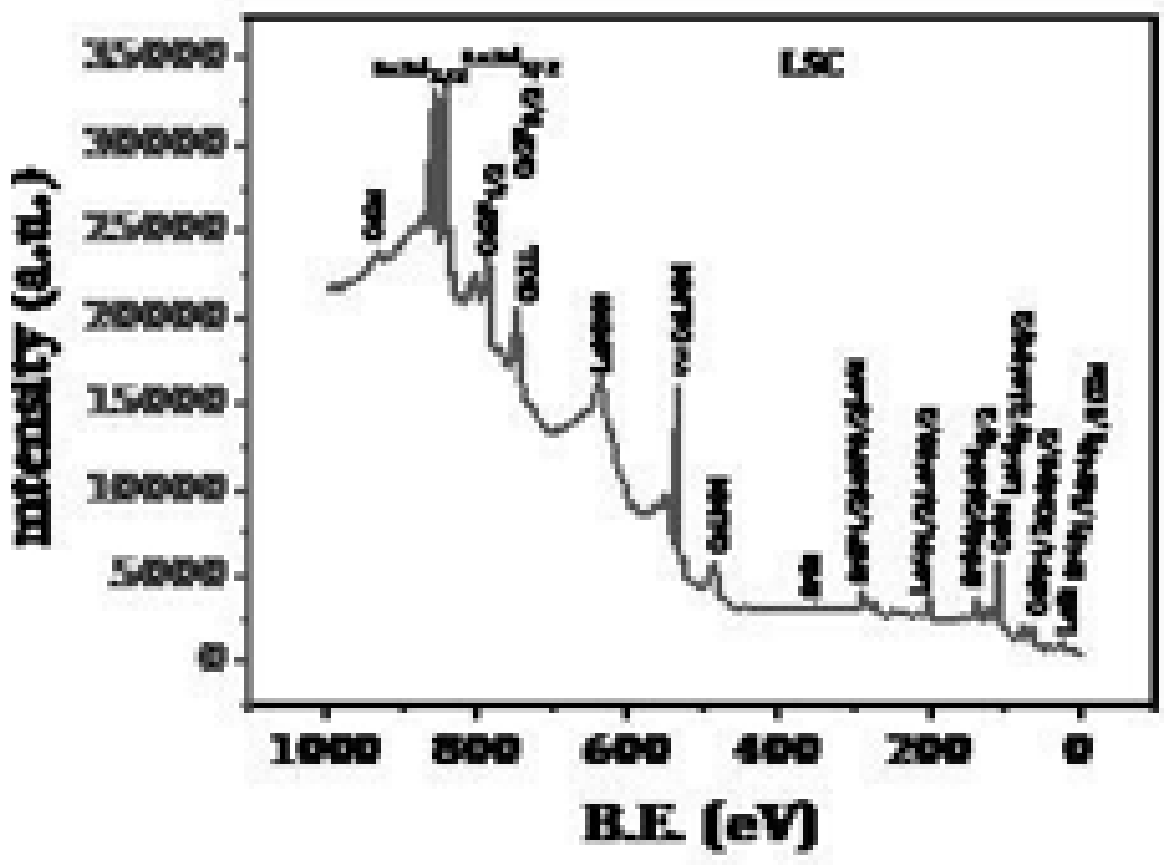

Figure 3. XPS spectrum of LSC

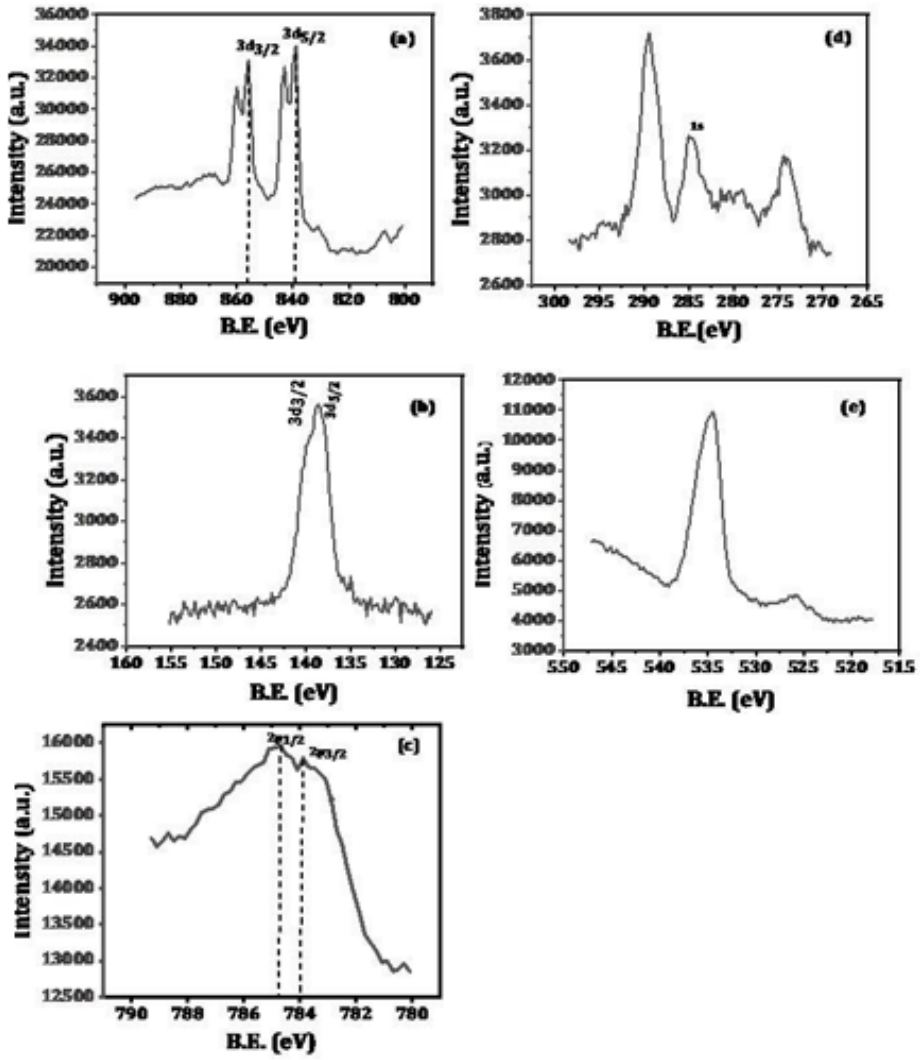

Figure 4. XPS spectrum of (a) La, (b) Sr, (c) Co, (d) C and (e) O

3.3 UV-Visible Spectroscopy

The UV-Visible absorption spectra of the LSC thin films are shown in Fig. 5. The figure clearly shows strong absorption in the ultraviolet region between 226 nm and 228 nm. No absorption bands are observed in the visible region between wavelengths 229 nm and 400 nm. According to UV-Vis spectrophotometer analysis, film absorption increases with increasing strontium concentration. It was observed that increasing the carrier concentration resulted in higher adsorption [17]. The following Tauc's formula has been used to calculate the band gap value,

$$(ah\nu)^{\frac{1}{\gamma}} = B(h\nu - E_g) \text{ ----} (1)$$

The band gap of LSC has been calculated by extrapolating the linear region of the plots $(\propto h\nu)^2$ vs. band gap energy.

As Sr^{2+} (Strontium) content increases, the band gap widens. This widening can be attributed to the Burstein-Moss effect [18]. With increasing doping concentration, donor states form, elevating the Fermi level. In degenerate doping, the Fermi level moves closer to the conduction band and lies above the occupied donor states. In a degenerate semiconductor, electrons can be excited only from the valence band to the conduction band above the Fermi level, because the donor states occupy all states below it. As a rfigesult, the band gap increases with higher strontium ion content, as shown in (Table2)

Table 2. Band Gap Energy

Peak	S. P. Area	Mean	S. D.	Mode
No	Ratio			
1	1	127.5 nm	54.8 nm	110.0 nm
2	----	----	----	----
3	----	----	----	----
Total	1	127.5 nm	54.8 nm	110.0 nm

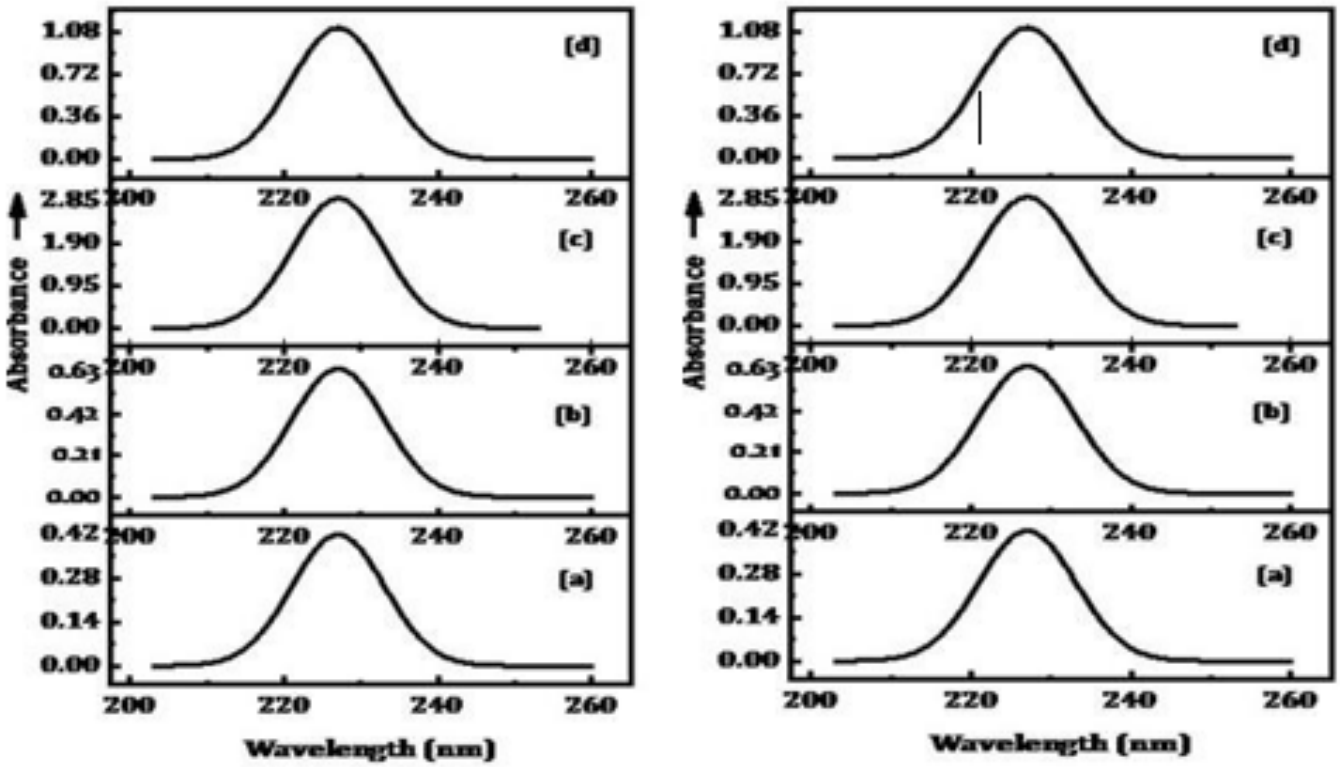

Figure 5. (a) Absorption spectra of LSC thin films (a) LSC91, b) LSC82, (c) LSC73, d) LSC64 (b) Band gap pattern (a) LSC91, b) LSC82, (c) LSC73, d) LSC64

3.4 D. C. Resistivity Measurement

The D.C. electrical resistivity of the LSC sample heat-treated at 1100 °C was measured using a two-probe technique. All samples exhibit a decrease in resistivity with increasing temperature, indicating semiconducting behaviour. At high temperatures, the resistivity remains nearly constant. This decrease with increasing temperature is attributed to an increase in thermally activated drift mobility of charge carriers, according to the hopping conduction mechanism [19].

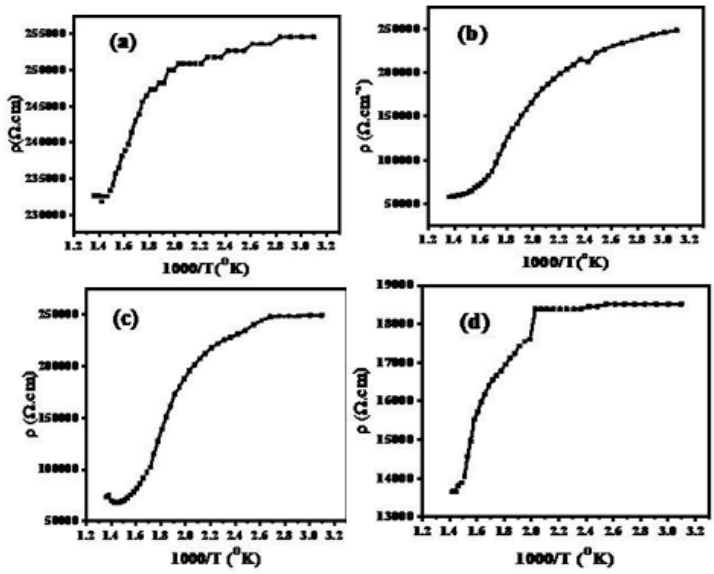

Figure 6. D.C Resistivity of LSC thin films (a) LSC91, b) LSC82, (c) LSC73, d) LSC64

3.5 Impedance Study

The variation of real and imaginary components of impedance with frequency for LSC samples at room temperature is shown in Fig. 5 (a) and (b). The value of Z' is higher in the low-frequency region, and it was found that as frequency increases, the value of Z' decreases slowly and attains a constant value in the high-frequency region. The variation of Z" with frequency revealed that Z" initially increases, and as the frequency further increases, its value decreases and attains a slightly constant value. This behaviour indicates the presence of space charge polarisation.

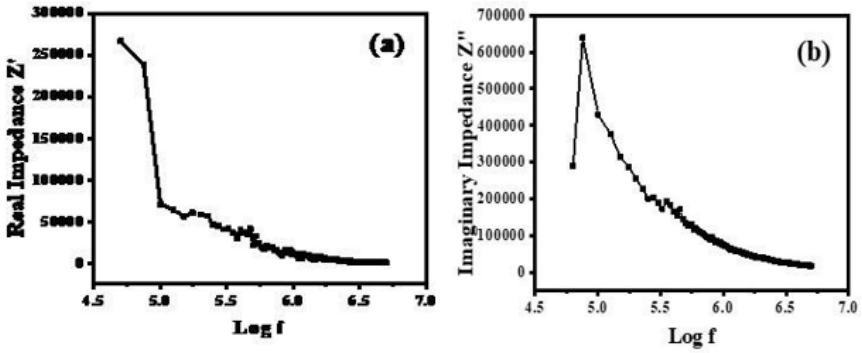

Figure 7. Variation of (a) real and (b) imaginary component of impedance as a function of frequency for LSC films

4. Conclusion

From XRD data, the confirmation of phase formation was done. By using the Tauc plot, semiconductor band gap analysis was done. From this graph, it was concluded that with increasing strontium, the band gap increases. From the resistivity graph, it was found that as the strontium content increases, resistivity decreases. The real and imaginary components of the impedance graph confirmed that the LSC samples exhibit semiconducting behaviour.

Compliance with Ethical Standards

- Disclosure of potential conflict of interest.
- Research Involving Human Participants.
- Informed consent.
- **Competing Interest**
- No funding was received to conduct this study.

Research Data Policy and Data Availability

Statements: All data generated or analyzed during this study are included in this published article.

Author Contribution

The author contributed to the study's conception and design. B. S. Kamble performed material preparation and data collection. B. S. Kamble wrote the first draft of the manuscript, and the co-author, Pranav B. Kamble, read, analysed, and approved the final manuscript.

References

1. Ozlu H, Ersoy, E, Cakar, S, Turkoglu, O (2010) The preparation and characterization of LaNi1-xFeXO3perovskite thin film as a cathode electrode for solid oxide fuel cell applications, 2nd International Conference on Nuclear and Renewable Energy Resources

2. Kongfa Chen, Zhe Lu, Xiangjun Chen, Na Ai, Xiqiang Huang, et al. (2007) Journal of Power Sources 172,

3. 748.

4. Tahir N N M, Baharuddin NA, Samat AA, Osman N, Somalu M R (2022) A review on cathode materials for conventional and proton–conducting solid oxide fuel cells, Journal of Alloys and Compounds 894, 162458.

5. Pesaran A, Jaiswal A, Wachsman ED (2019) Bilayer electrolytes for low temperature and intermediate temperature solid oxide fuel cell-A review Energy Storage and Conversion Materials 1-41

6. Ortiz-Vitorianoa N, Ruiz de Larramendia I, Ruiz de Larramendia JI, Arriortuab MI, Rojo T (2011) Journal of Power Sources, 196: 4332-4336

7. Alder SB (2000), Solid State Ionics 111,135: 719-725

8. Badwal SPS, Jiang SP, Love J, Nowotny J, Rekas M, et al. (2001) Ceram Int 27: 419–429.

9. Mehdi AM, Hussain A, Song RH, Lim TH, Kazmi WW, et al. (2023) RSC Adv 13: 25029–25053.

10. Hjalmarsson P, Sogaard M, Hagen A, Mogensen M (2008) Solid State Ionics 179: 636.

11. Ajmal S, et al. (2019) J Mater Res Technol 8(5): 4831.

12. Zuev AY, Sareda VV, Tsvetkov DS (2012) J Electrochem Soc 159: F594.

13. Rupp G, Limbeck A, Kubicek M, Penn A, Stoger-Pollach M, et al. (2014) J Mater Chem A 2: 7099.

14. Adler SB (2004) Chem Rev 104: 4791.

15. Zhao F, Peng R, Xia C (2008) Fuel Cells Bulletin 12.15. Tsuji Y, Sako S, Nitta K, Yamamoto K, Shao-Harn Y, et al. (2020) Solid State Ionics 317: 115502.

16. Deng J, Zhang L, Dai H, He H, Au CT (2008) Ind Eng Chem Res 47: 8175–8183.

17. NicDaeid N (2019) Forensic Sciences: Systematic Drug Identification. Elsevier, 75–80.

18. Ivchenko V (2024) Phys Scr 99: 035952.

19. Khetre SM, Jadhav HV, Jagdale PN, Kulal SR, Bamane SR (2011) Adv Mater Sci Res 503.